Determination of the critical field and critical temperature for various Type I and Type II metals and alloys

Alexander Nie and Mobolaji Williams
Harvard University, 77 Massachusetts Ave., Cambridge, MA 02138
(Dated: February 28, 2016)

This experiment illustrated the main characteristics of type I and type II superconductors (SCs), namely the fall off of resistance below a critical temperature and the expulsion of net magnetic fields below a critical magnetic field at that temperature. We also demonstrated how type II SCs are distinguished from type I SCs by the partial penetration of magnetic fields into the interior of type II SCs when they are above a first critical field value but below a second critical field value. We confirmed the superconducting properties and types of various known samples (Pb, In, Sn, In_2Bi, In_4Bi) by studying them near their superconducting regime and by plotting their susceptibilities as a function of applied field and resistances as a function of temperature. The critical magnetic field as a function of temperature was also plotted, for each sample, and was found to reproduce the characteristic quadratic behavior. This in turn allowed us to determine critical temperature and zero-temperature critical field for each sample. For lead, for example, we found a critical temperature of 7.24 ± 0.04 K and a zero-temperature critical field of 810 ± 10 G, which compared well to the literature values [1] $T_c = 7.196 \pm 0.006$ and $H_c(0) = 803 \pm 1$ G. These measurements were repeated on the sample SnPb (with unknown conducting properties), and it was found to have behavior similar to what we expect from a type II SC.

I. INTRODUCTION

Superconductivity refers to two related phenomena in materials. First, superconductors are perfect electrical conductors; that is, they have zero electrical resistance. Second, superconductors exhibit the Meissner effect, in which they expel all magnetic fields from their interiors. Initially discovered in 1911 by Dutch physicist Heike Kamerlingh Onnes, superconductors remain a developing field of study in both application as well as theory. A brief overview of the history of the subject follows.

Superconductivity, and more specifically, perfect conductivity, was first discovered by Onnes [2] during an experiment to measure the dependence of resistance on temperature in low-temperature mercury. At the time, some physicists, such as Lord Kelvin, postulated that near 0 K, electron flow would come to a halt, thereby forcing materials to become perfect resistors. Others, such as Onnes, believed resistance would dissipate given its inverse relationship with temperature, leading to perfect conductors. The latter was confirmed in 1911 when upon cooling mercury to 4.19 K, Onnes noted a sudden drop in the resistance to nearly zero. In 1912, upon passing a battery-generated current through the mercury, Onnes noted that after disconnection of the battery, the current remained at the same intensity, indefinitely. Other examples of perfectly conducting materials were found shortly after, including lead in 1913.

In 1933, Walther Meissner and Robert Oschenfeld [3] observed the second property of superconductors: the expulsion of applied magnetic fields by measuring the magnetic flux around low-temperature tin and lead samples. Phenomenological explanations followed. In 1935, Fritz and Heinz London gave a phenomenological explanation of superconductivity using what are now known as the London equations. In this model, applied magnetic fields inside a superconductor exhibit exponential decay within a characteristic distance from the material's surface, known as the London penetration depth. In 1950, physicists Lev Landau and Vitalij Ginzburg proposed another phenomenological explanation, which became what is now known as the Ginzburg-Landau theory of superconductivity. Based on Landau's theory of second-order phase transitions and the Schrdinger-like equation, the theory succeeded in macroscopically describing superconductivity arising from quantum mechanical effects. Finally, in 1957, John Bardeen, Leon Neil Cooper, and John Robert Schrieffer proposed a physical explanation for superconductivity, which became known as BCS theory. In this model, superconducting currents arise from the migration of electron pairs, known as Cooper pairs, formed by electron-phonon interactions within a crystal lattice. Further developments included the discovery of type I and II superconductors, discussed later in the theoretical background section, as well as high temperature superconductors, which are beyond the scope of this experiment.

In Sec. II, we review the various physical explanations for superconductivity starting from the London equations and concluding with the BCS theory. We also discuss the differences between type I and type II superconductors as such differences are relevant for our experiment, and explain how the emf that we measured with the lock-in amplifier is related to susceptibility. In Sec. III, we outline the apparatus we used in the experiment along with the various signal manipulation procedures we employed to extract Meissner effect and resistivity measurements. In Sec. IV we present the zero-temperature critical field and critical temperature values for all the superconducting samples and the plot of resistivity of SnPb as a function of temperature. In Sec. V we discuss the possible sources of error in our results. In particular we com-

ment on the possible superconducting type of SnPb and explain why our results are inconclusive in this regard.

II. THEORETICAL FOUNDATIONS

A. London Theory

In 1935 [4], F. and H. London postulated what is now known as the London equations to obtain a phenomenological theory of a superconductor. The equations were

$$\dot{\vec{J}} = \frac{ne^2}{m}\vec{E} \tag{1}$$

$$\vec{B} = -\frac{m}{ne^2}\vec{\nabla}\times\vec{J}, \tag{2}$$

where e is the electric charge of the electron, m is the mass of an electron, and n is the density of electrons within the superconductor. Eq.(1) follows from the observed zero resistance in a superconductor, and Eq.(2), although seemingly related to the first through Faraday's and the Amper-Maxwell Laws, must be postulated independently to describe the Meissner effect. With regard to the Meissner effect, by taking the curl of Eq.(2) and using the Ampere-Maxwell Law we obtain

$$\vec{\nabla}^2\vec{B} = \frac{1}{\lambda_L^2}\vec{B} \tag{3}$$

where $\lambda_L \equiv \sqrt{m/\mu_0 ne^2}$ is termed the London penetration depth. The solution to Eq.(3) for the interior of a superconductor yields with (B constant along the boundary and going to zero at infinity) an exponentially decreasing magnetic field consistent with the observations of Meissner.

B. Landau-Ginzburg Theory

For the Landau-Ginzburg (LG) [5] model one assumes we have a complex valued order parameter ϕ which has a potential $V(\phi) = a|\phi|^2 + b|\phi|^4$ and which interacts with an electromagnetic field through a gauge covariant derivative $\nabla_j = \partial_j - 2ieA_j$. The vector potential itself contributes a free energy arising from the magnetic field strength term. In all the free energy density of the system is

$$\mathcal{H} = -\frac{1}{2\mu_0}B_j^2 + \frac{1}{2m}|\nabla_j\phi|^2 + a|\phi|^2 + \frac{b}{2}|\phi|^4 \tag{4}$$

where for simplicity we take the electric field to be zero

The crucial physical assumption Landau and Ginzburg made was to take a to be proportional to $T - T_c$. The result was that the ϕ which minimizes $V(\phi)$ is either zero or non-zero contingent on what T is relative to T_c, and the resulting equations of motion for A_j and hence the magnetic field B_j change analogously.

The Landau-Ginzburg model was in a way a phenomenological extension one level deeper than the London Equations. But, like the London Equations it is limited by its conceptually motivated formalism. For example, it "explained" the Meissner effect and was able to derive the current-field relations which led to it, but the postulation of the model itself, beyond the existence of the electromagnetic potential, had little physical motivation. Moreover, the model could not predict T_c or explain the electron pair bonding in superconductors.

C. BCS Theory

The first microscopic theory of superconductors, was the Bardeen-Cooper-Schrieffer (BCS) [6] theory. In the BCS theory, electrons of opposite momentum and opposite spin form spin singlet pairs termed (Cooper pairs) which propagate through the superconducting lattice like bosons. It is the cooper pairs which make up the current which flows without resistance. The specifics of BCS theory are not important for our experimental analysis, but it is worth mentioning that the first quantum mechanical model for superconductivity was developed in 1957, more than 40 years after Onnes discovered the first superconductors.

D. Type I and Type II Superconductors

One of the fundamental properties of all superconductors is that when they are in their superconducting phase, below a certain applied magnetic field strength (i.e., $H < H_c$), net magnetic fields (that is B) are completely expelled from their interior. Type I SCs refer to metals which are characterized by a single critical magnetic field, below which the metal completely expels magnetic fields and above which the metal returns to its normal conducting phase provided the metal is below its superconducting critical temperature throughout. A schematic plot of the magnetization as a function of applied field for a type I SC is shown in Fig. 1a.

Type II SCs refer to metals which are characterized by two critical magnetic fields. Below the lower critical field, the metal exhibits complete expulsion of magnetic fields. Between the two critical fields the metal exhibits partial expulsion of magnetic fields, and above the higher critical field the sample returns to its normal conducting phase. A schematic plot of the magnetization as a function of field for a type II superconductor is shown in Fig. 1b. For type II SCs, although the magnetic field exhibits partial expulsion between the two critical field values, the resistivity still remains zero in this field regime.

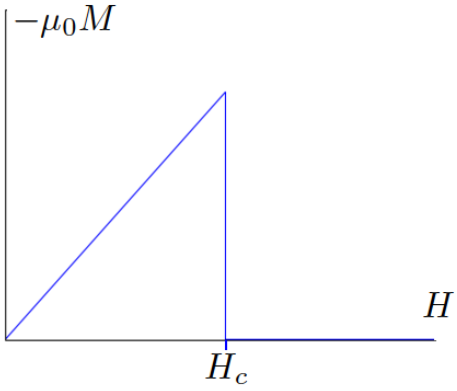

(a) Type I Supeconductor

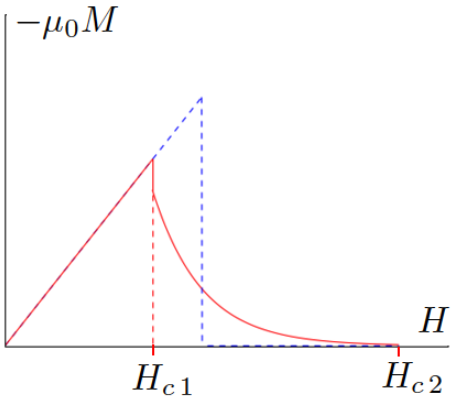

(b) Type II Superconductor

FIG. 1: Magnetization vs. field for superconductors: Type I superconductors are characterized by a single critical magnetic field above which the Meissner effect disappears. Type II superconductors are characterized by two critical magnetic fields. Above the first field, there is partial magnetic field expulsion and above the second field the metal returns to its normal state. We note for the type II SC, $\partial M/\partial H$ is theoretically infinite at $H = H_{c1}$. Based on figures in [7].

E. EMF and Susceptibility

The critical magnetic field of a sample (metal or alloy) can be determined by plotting the magnetization or susceptibility of the sample as a function of field and observing whether it exhibits either of the canonical diamagnetism behaviors depicted in Fig. 1. However, for this experiment we did not have a direct means of measuring magnetization and instead measured the emf generated by each sample and used this emf measurement as a proxy for susceptibility (and thereby magnetization).

The relationship between the susceptibility and the emf of a sample can be established through basic electromagnetism. In what follows we ignore the vector nature of the fields because we are only interested in their values along a single axis. Say we have the sample configured as shown in Fig. 3. The sample is immersed in an applied magnetic field $H(t)$ which is changing in time. This time dependent *applied* magnetic field leads to a time dependent magnetic field which by Faraday's law produces an emf in the surrounding coil of wire. This emf can be written in terms of the susceptibility of the sample.

Mathematically, we begin with the definition of the magnetic flux density in terms of the applied magnetic field and the magnetization: $B = H + \mu_0 M$. Differentiating this equation, using the chain rule, and applying the definition of susceptibility as $\chi = \partial M/\partial H$, we find

$$\frac{dB}{dt} = \frac{dH}{dt}\left(1 + \mu_0 \chi\right). \tag{5}$$

For this experiment, the applied magnetic field was swept linearly in time from 0 to some $H_{\max}$ over a time τ. So the time derivative of the applied field can be written generally as $dH/dt = H_{\max}/\tau$. Also, by Faraday's law we know the emf generated by the changing magnetic field is

$$\mathcal{E}_{\text{out}} = -A\frac{dB}{dt} \tag{6}$$

where A is the cross sectional area of the sample. Substituting Eq.(5) into Eq.(6), we then obtain

$$\mathcal{E}_{\text{out}} = -A\frac{H_{\max}}{\tau}(1 + \mu_0 \chi). \tag{7}$$

Our desired relation between the emf and the susceptibility. For this experiment, we directly measure the left-hand side of Eq.(7) and then infer the properties of the right-hand side.

Although a possibly more complete analysis would have us exactly computing the susceptibility (and through integration, maybe even the magnetization) of each sample, for the purposes of our analysis it sufficed to only identify the field values where the susceptibility was singular or where it began to asymptote to a constant value. Thus we were not primarily interested in the absolute value of the susceptibility but in its functional behavior, and such behavior is independent of proportionality constants or vertical shifts. Therefore, the emf, by its relation to susceptibility established in Eq.(7), proved to be adequate for our analysis.

III. EXPERIMENTAL BACKGROUND

A. Apparatus

1. *Cryostat*

A schematic diagram of the cryostat (Janis 8DT) is shown in Fig. 2. Samples to be cooled are situated in an isolation chamber which is insulated by vacuum from

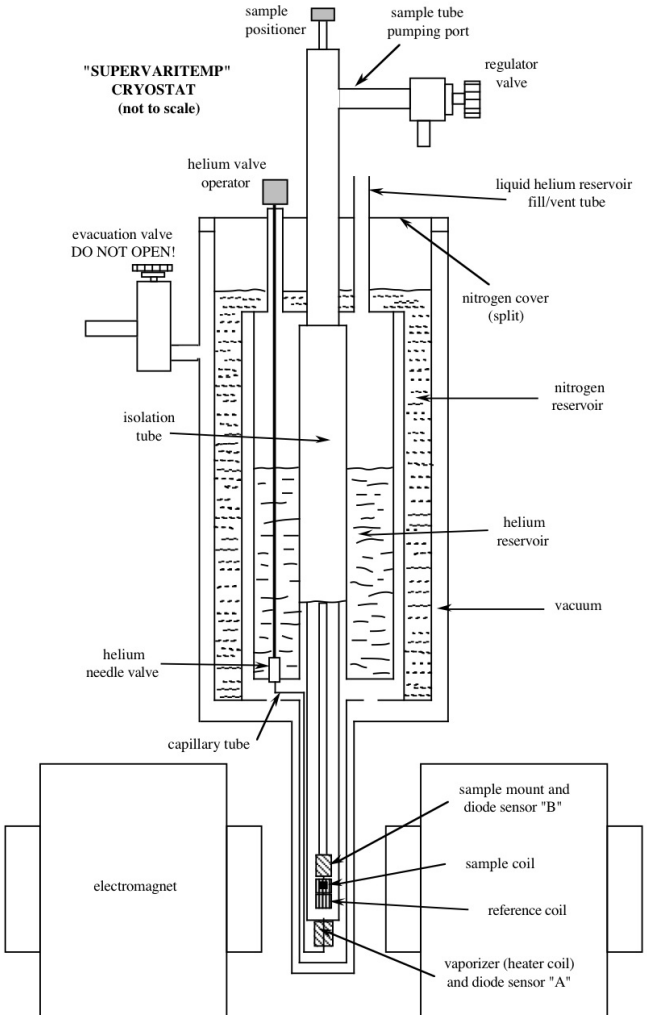

FIG. 2: Janis 8DT cryostat: Experimental setup for cryostat and samples. The samples are at the bottom of the cryostat in a region of nonzero magnetic field. In the main body of the cryostat, separate cylindrical spaces filled with liquid helium and liquid nitrogen function to cool the sample region to the low temperatures ($\sim \mathcal{O}(1\text{ K})$) needed to demonstrate the effects definitive of superconductivity. Figure taken from lab benchnotes.

a surrounding helium bath. This helium bath is then insulated by vacuum from a surrounding liquid nitrogen bath, which itself is insulated from room temperature by vacuum. A valve controls the flow of helium from the helium reservoir into the isolation tube while a vacuum pump creates a pressure gradient to draw helium into the isolation tube. The cryostat contains two temperature-sensing diodes "A" and "B"; the former sits outside the isolation tube on the heating coil, while the latter sits above the samples inside the isolation tube.

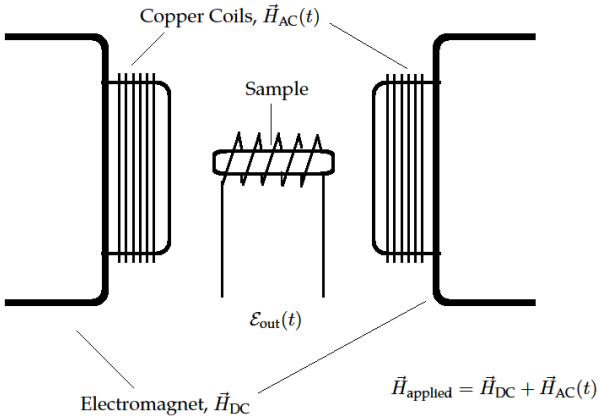

FIG. 3: Setup of electromagnet: The cylindrical samples were arranged along an axis parallel to the direction of the applied magnetic field $\vec{H}_{\text{applied}}$. The net applied field had two contributions: a time-dependent field, $\vec{H}_{\text{AC}}(t)$ arising from the alternating-current run through copper wires arranged in a solenoid; a constant field $\vec{H}_{\text{DC}}$ generated by iron pole pieces (the electromagnets in the figure). The constant magnetic field allowed us to directly control the magnetic field applied to the samples, while the time-dependent magnetic field generated an emf, $\mathcal{E}_{\text{out}}(t)$, in the coil wrapped around the sample which could then be used to infer whether the sample was expelling the external magnetic field. This in turn allowed us to determine whether the sample was superconducting. Figure created by authors.

2. Electromagnet

As shown in Fig. 3, the electromagnet consisted of iron cylindrical pole pieces extending towards the samples. While the larger outer iron cores supplied a constant magnetic field generated by the direct current, copper coils wrapped around the inner iron cores supplied a time-dependent oscillating magnetic field generated by an alternating current. The the constant magnetic field was directly controlled by a current source and thus served as the field varied to move the samples into and out of their superconducting field regimes. The time-dependent magnetic field generated an emf in the coil of wire wrapped around each sample, and thus by Eq.(7), allowed us to determine whether the sample was in its superconducting phase.

B. Methods

1. Samples

Cylindrical samples (16mm long x 1mm diameter) of tin, lead, a 40% lead alloy of tin-lead, indium, two indium alloys doped with 2% and 4% bismuth, copper, and

Teflon were held within the same sample holder of the cryostat. Pickup coils of copper wound on the samples all contain 240 turns of #40 varnished magnet wire in two layers. Within the superconducting regime, the expulsion of applied magnetic fields reduces the magnetic flux in the pickup coils, resulting in a nearly-zero induced emf in the coils whereas in the normal regime, applied magnetic fields generate induced emf in proportion to field strength.

2. Cooling

Cooling was accomplished using liquid and vaporized helium. After an initial liquid helium transfer into the cryostat (Janis 8DT, 7854), a pressure gradient was set up using the vacuum pump (Alcatel) to draw helium into the isolation chamber when the control valve was open. Cooling to around 4.5 K was accomplished by only allowing vaporized helium into the isolation chamber. Due to uneven heating, care was taken to proceed by only lowering, rather than raising, temperatures between experimental runs. For cooling below 4.2 K, the boiling point of helium, the samples were immersed in liquid helium by allowing liquid into the isolation chamber. Rather than using the temperature controller, temperature measurements were then taken by pressure gauges of the cryostat, which measured the pressure of vaporized helium in the chamber. A calibration table [8] was then used to convert measured helium pressures into temperatures. To ensure that pressure readings were relevant (i.e., that liquid helium did not fill the chamber completely), a liquid helium level meter (Model 110, American Magnetics Inc.) was used to detect the amount of liquid helium in the chamber.

3. Meissner Effect

In overview, measurement of the Meissner Effect in various samples was accomplished by cooling the samples to various low-temperatures, sweeping the applied magnetic field strength, reading the induced electromotive force into LabVIEW, and converting this induced electromotive force into an induced susceptibility through Eq.(7).

First, the cylindrical samples were wrapped in copper coils and placed into the cryostat chamber so that the cylindrical axis was parallel to the applied magnetic field lines. Following a liquid helium transfer, the samples were cooled to around 9 K using the vacuum pump mechanism described earlier, with temperature being monitored by the temperature controller. In order to ensure that samples equilibrated with the helium bath, the next stage of the experiment was delayed until temperature readings at diode sensor B agreed with the desired temperature and held constant for at least 30 seconds. This was seen as a more accurate reading than diode sensor A, which was not located in the helium bath near the samples.

The gaussmeter (Model 615, Bell Inc.) was initially zeroed to an accuracy within 1 gauss or 1 G. The probe of the gaussmeter measured the magnetic field through the Hall effect. Alternating magnetic field was applied through a power source (BOP 20-5M, KEPCO) and function generator (Model 21), followed by placement of the gaussmeter probe between the two iron cores of the cryostat's electromagnet. The probe was then rotated until a maximum reading for the applied magnetic field was found, indicating it was oriented perpendicularly to the field. Subsequently, the alternating field was calibrated to provide a sinusoidal signal with an amplitude of 60 G at 23 Hz, where frequency was chosen to avoid interference from the standard 60 Hz supplied by electronics in the surrounding environment. Finally, the lock-in amplifier (SR530, Stanford Research Systems) was connected at 50 nanovolt sensitivity to read the induced emf and send an amplified signal to LabVIEW for recording.

To sweep the magnetic field, a DC source was created by a second power source (BOP 20-20 M, KEPCO) and a function generator (AFG 3022B, Tektronix), which provided a triangular wave signal. One-period sweeps were then conducted from 0 V to 4V on the function generator at 50 mHz with a manual trigger, and results saved into the LabVIEW program. These sweeps were repeated at intervals of 0.5 K from 5.5 to 8 K for Pb and SnPb and 6 to 1.5 K for the rest of the samples, as Pb and SnPb exhibit the transition at a much higher temperature than the other samples.

4. Resistivity Measurement

The resistivity measurements were performed solely on the SnPb sample. Using the BOP 20-20 M power source and a voltmeter, a 4-point voltage measurement was taken across the SnPb sample in series with a 50 MΩ resistor at 66 μ A, 100 μ A, and 133 μ A. This setup was then repeated in increments of 0.5 K from 5.5 K to 8.5 K.

IV. EXPERIMENTAL ANALYSIS

A. Magnetic Field Calibration

The LabVIEW display units of the applied magnetic field were not in physical units, so a calibration had to be performed. For this calibration we swept the magnetic field from 0 G to a known field $H_{\max}$ as measured by the gaussmeter probe. We displayed this applied magnetic field on the LabVIEW output throughout the sweep and were thereby able to determine which LabVIEW units corresponded to a field of 0 G and a field of $H_{\max}$. We repeated this calibration twice, and with the assumption of a linear relationship between kG (true magnetic

field units) and the LabVIEW units, we obtained a function which converted from LabView units to kG. The uncertainty in the magnetic field as read from LabVIEW yielded an uncertainty of 10 G for all our measurements.

B. Voltage Calibration

Similar to the magnetic field reading, the LabVIEW display of the voltage across the sample was not in physical units, so a calibration had to be performed, as described earlier. Assuming that the LabVIEW program merely converted from one unit scale to another, we assumed a linear model and performed a linear regression on the data.

C. Meissner Effect: Determining the Critical Field

In this section we discuss how we determined the critical magnetic field for each sample.

While the temperature of the system was controlled using the cryostat and was directly measured using a pressure gauge and/or heater-thermostat, the critical magnetic field had to be determined from how the produced emf varied as we linearly swept the applied field from zero to some maximum value well above the transition field. Specifically we referred to the theoretical curves in Fig. 1a.

The critical field for a type I superconductor was straight forward to determine. By Fig. 1b we expect the susceptibility to have a singularity at the critical field above and below which the susceptibility is constant (since the derivative of $M(H)$ is zero). Eq.(7) implies we should see a singularity in the measured emf at the same critical field value of the susceptibility. Thus for type I superconductors, the critical magnetic field was defined as the field yielding the highest emf value with an error taken to be half the width of the singularity peak. Such a singularity is depicted for Lead at 5.08 K (i.e. well below the determined superconducting temperature) in Fig. 4a. For most measurements this error amounted to about 0.01 kG.

For type II superconductors, according to Fig. 1b we expect the emf (again by Eq.(7)) to have a singularity at the first critical field value. Above this critical field value, instead of the the emf returning to a constant value, we expect it to increase as a function of applied field (in the region $H_{c1} < H < H_{c2}$), before leveling off. The second critical field value was defined as the field value at which the emf had stopped increasing and had leveled off to a constant value. An example of such a plot is shown in Fig. 4b The error for the first critical field was determined by taking the half width of the singularity peak. The error for the second critical field was taken categorically to be 0.01 kG, as an estimate.

D. Meissner Effect: Critical Field as a Function of Temperature

A major goal for this experiment was the determination of the critical field at zero temperature and the critical temperature for each superconducting sample. The Cu and PTFE samples did not exhibit the behavior shown in Fig. 4 and hence were determined to be non-superconducting and were eliminated from subsequent analyses. For the remaining samples, the critical magnetic field was determined as outlined in Sec. IV C. Also, by our magnetic field calibration explained in Sec. IV A, our critical magnetic field measurements retained an error of 10 G. The critical temperature was measured with the Lakeshore Temperature Controller for temperatures above 4 K and was measured with the Cryostat pressure gauge for temperatures below 4 K. In both cases, there were uncertainties in the temperature measurement which amounted to deviations of about 0.1 K from the recorded result.

By [9], the experimental fit for the functional relationship between critical magnetic field and critical temperature was found to be a quadratic polynomial of the form

$$H_c(T) \approx H_c(0)\left(1 - \frac{T^2}{T_c^2}\right). \tag{8}$$

With $H_c(0)$ and T_c as fitting parameters, we used this function as a fit for our data. As a goodness-of-fit estimate we computed the reduced-χ^2 for each fit against its corresponding data. The critical field vs. critical temperature for all the superconducting samples, their associated fits, and the reduced-χ^2 statistics are shown in Fig. 5. Because some books use various conventions we mention the reduced-χ^2 statistic we used for our fits. Our χ^2/ν was defined as [10]

$$\chi^2/\nu = \frac{1}{\nu}\sum_i \frac{1}{\sigma_i^2}\left[H_{c\,i} - H_c(T_i)\right]^2. \tag{9}$$

where the sum runs over each data point, T_i is the measured temperature, $H_{c\,i}$ is the measured critical field, σ_i is the uncertainty in the critical field measurement, and $H_c(T)$ is given by Eq.(8). ν is the number of data points minus the number of parameters for the fit; it was 5 for each of the fits in Fig. 5.

Using Eq.(8) as a fit in turn allowed us to estimate the critical field at zero temperature and the critical temperature for each sample. For most of the samples, the exact fitting parameter values for $H_c(0)$ and T_c were obtained using Python's `optimize.curvefit` [11] algorithm and their corresponding errors were defined as the square root of the diagonal elements of the associated covariance matrix. For the type II SCs, there were two parabolic curves defining the phase diagram (one for each H_c), and thus there were two fitting parameter predictions for the critical temperature. We averaged the two predictions to estimate the critical temperature for the sample, and used

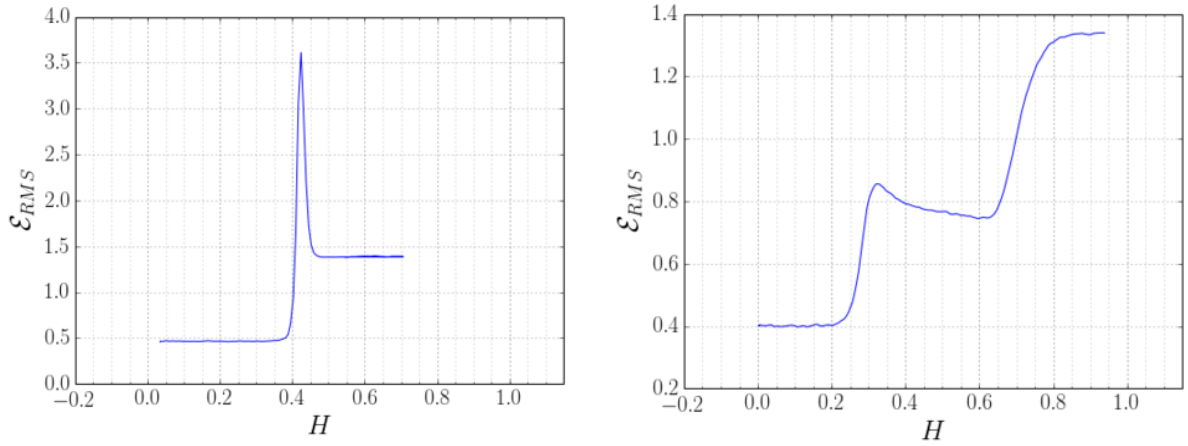

(a) Pb at 5.08 K

(b) In_4Bi at 1.52 K

FIG. 4: RMS-emf as a function of field (in G) for various samples in superconducting regime. Plots such as these were used to determine the critical magnetic field of various samples using intuition extrapolated from the theoretical plots in Fig. 1. The exact scale of the y-axis was not important in the analysis as it was only the singular and asymptotic behaviors of the curves which determined the critical fields.

the individual results to establish bounds on the estimate. This lead to a larger critical temperature error for the type II SCs than for the type I SCs. The results of these analyses are shown in Table I.

The estimates of H_c and T_c were determined from the nonlinear fit implemented through python's curve fit module. The fitting equation was Eq.(8). In particular for Type II superconductors we assumed Eq.(8) applied to both H_{c1} and H_{c2} curves. The critical temperature T_c for these type II SCs was computed as an average of the critical temperature for each H_c curve. The errors were determined by the bounds established by each predicted critical temperature and thus were larger than the corresponding bounds for the type I SCs.

E. Perfect Conductivity: $R(T)$ measurements

Using our voltage calibration and Ohm's Law, the voltage drop across the SnPb sample, as recorded on LabVIEW, was first preprocessed to give the corresponding resistances of the samples at various temperatures and currents. As the models guiding the experiment assumed superconductivity was a sudden transition, a sigmoidal curve was used to fit the data. The inflection point of the sigmoidal curve was then taken to be the transition point, whose corresponding x-value was the transition temperature. The results are given in Table II with the averaged result yielding a transition temperature of $(7.46 \pm .05)$ K and uncertainties given as one standard deviation.

Using the results of the voltage calibration experiment and Ohm's Law, the voltage drop across the SnPb sample as recorded on LabVIEW was first preprocessed to give the corresponding resistances of the samples at various temperatures and currents, as shown in Fig. 6 As the models guiding the experiment assumed superconductivity was a sudden transition, a sigmoidal curve was used to fit the data, as common when modeling step functions. The inflection point of the sigmoidal curve was then taken to be the transition point, whose corresponding x-value was the transition temperature. The results are shown below, with the uncertainties given as one standard deviation. The results are given in Table II, with the averaged result yielding a transition temperature of $7.46 \pm .05$ K.

V. DISCUSSION

The zero-temperature critical field and critical temperature values listed in Table I are the main results of the Meissner Effect portion of this experiment. For the type I SCs, comparing our predictions to the standard values found in the CRC Handbook of Chemistry and Physics [1], we find that the known the critical field and critical temperature values for our metals fall within our predicted range, except for the the zero-temperature critical field predictions for indium and tin. There seems to be no ready reference for the type II SCs, but seeing as the singularity peaks were wider for the type II SCs we can assume the possibility for error in determining the first critical magnetic field was greater than for the type I determination. Moreover, the second critical field for type II SCs was not determined by a singularity but rather imprecisely by locating the field value at which the emf reached a constant value. Thus throughout the experiment, the values of the critical field were determined by inspection of the emf vs. H graph (such as those shown in Fig. 4) and such inspection, done by "eye", is inevitably subjective and prone to error.

Also, the fits and their associated χ^2/ν values

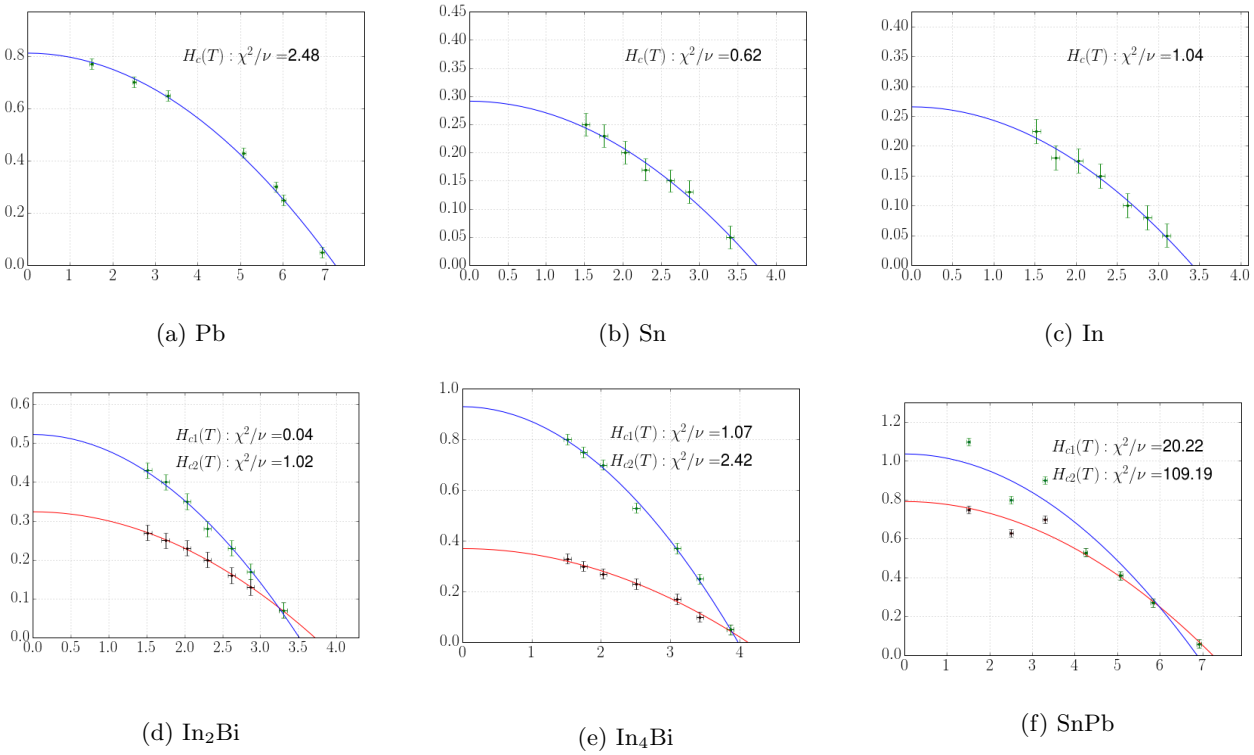

(a) Pb (b) Sn (c) In

(d) In_2Bi (e) In_4Bi (f) SnPb

FIG. 5: Critical magnetic field (in kG) as a function of temperature (in K) for all the samples: We fit our collected critical field and critical temperature data to Eq.(8) for both type I and type II superconductors. For each fit we computed the reduced chi-squared as a goodness of fit measure and used the fit parameters $H_c(0)$ and T_c to estimate the critical field (at zero temperature) and critical temperature respectively of each sample.

TABLE I: Critical Temperature and magnetic field for studied samples. Presented as "Measured / Accepted Value", where the "accepted value" (when it exists) is taken from [1]. The errors are"one-standard deviation" errors. The Cu and PTFE samples are not listed because they are non-superconducting.

	Critical Temperature (K)	Critical Field(s) (G)		
Sample	T_c	$H_c(0)$	$H_{c\,1}(0)$	$H_{c\,2}(0)$
Pb	7.24 ± 0.04 / 7.196 ± 0.006	810 ± 10 / 803 ± 1	–	–
Sn	3.75 ± 0.07 / 3.722 ± 0.001	290 ± 10 / 305 ± 2	–	–
In	3.42 ± 0.06 / 3.408 ± 0.001	265 ± 10 / 281.5 ± 2	–	–
In_2Bi	3.6 ± 0.1 / 5.65	–	320 ± 10	520 ± 10
In_4Bi	4.1 ± 0.1	–	370 ± 10	930 ± 10
SnPb	7.0 ± 0.2	–	790 ± 10	1030 ± 10^a

[a]This value is contingent on a particular interpretation of the SnPb's susceptibility plot. Without this interpretation we must ignore this value and take SnPb to be a type 1 super conductor.

presented in Fig. 5 reveal that some critical field/temperature predictions are less reliable than others. In general [10], the closer χ^2/ν is to 1, the more reliable the fit. If χ^2/ν is much larger than 1 then the fit is not at all reliable, and if it is much less than 1 then it is possible that the fit is reliable or that we overestimated the uncertainty of our data points. Fig. 5 suggests the fits for SnPb are not at all reliable and hence we cannot trust the zero-temperature critical field or critical temperature predictions in Table I. The fits for the other metals/alloys are much closer to 1, and hence should yield predictions for $H_c(0)$ and T_c which are experimentally reliable.

The unknown sample SnPb yielded the least reliable

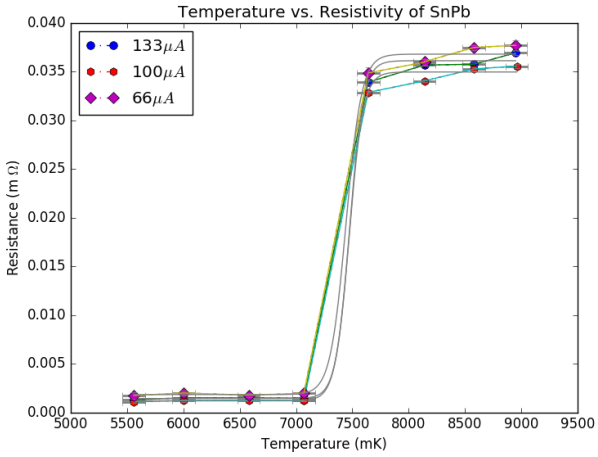

FIG. 6: Resistivity as a function of temperature in SnPb. To estimate the transition temperature, a sigmoidal fit was used, as a step-like function was expected (with slight slopes in the normal regime due to ohmic heating.

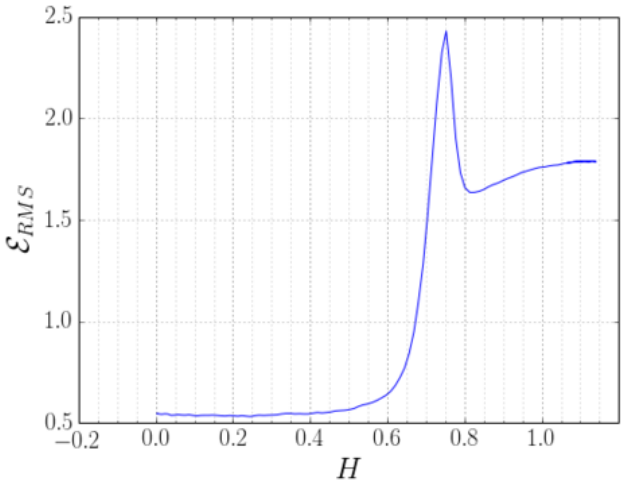

FIG. 7: SnPb at 1.52 K. Although the first critical field can be identified by the peak in the emf, the second critical field (if it exists) is more difficult to determine as it is not as prominent as that in Fig. 4b

TABLE II: Critical Temperature vs. Current for SnPb Sample

Current (μA)	$T_c(K)$	error (K)
66	7.448	.0912
100	7.467	.0813
133	7.453	.0857

fits to Eq.(8). One possible reason for its high χ^2/ν values was the ambiguous behavior of the emf vs. H plots used to determine the critical magnetic fields. Although SnPb clearly exhibited superconducting behavior, and the fact that it was an alloy suggested that it be a type II SC, it was difficult to distinguish the first critical field from the second critical field for much of the measured temperature range near 7.2 K. Moreover, when we finally reached a temperature where the two critical fields were better distinguished, it was not clear whether the behavior we observed was a feature of a type II SC or an artifact or our sweeping speed, noise, or some other systematic error. An example of one of the ambiguous plots of the emf generated by SnPb is shown in Fig. 7. The experiment was concluded after this ambiguity was noticed so measurements could not be performed again. So although it is clear that SnPb is a superconductor, in order to firmly determine its type, the analysis in this paper would need to be performed again on the sample perhaps with a slower magnetic field sweep and with a focus on temperatures well below the estimated critical temperature, 7.2 K.

For the temperature-dependence of resistance in SnPb, the critical temperature found was $7.46 \pm .05$ K, with 68% confidence. Although this confidence interval does not overlap the result obtained in the Meissner Effect experiment, a closer analysis of the modeling assumptions offers insight into the seemingly significant difference. First, a sigmoidal fit was used to model the data for the low-temperature resistance data. Although this model generally captures the sudden transition of the observed phenomena, it does not capture the behavior at higher temperatures. That is, while the sigmoidal function asymptotically levels off, the data at all three currents has a positive slope at temperatures higher than the transition, resulting in consistently positive residuals for high-temperature data points. The continued increased of resistance can be attributed to the behavior of SnPb in its non-superconducting regime, where its resistance is positively correlated with the temperature. Viewed through systemic error analysis, this causes the sigmoidal fit to exhibit a positive bias as it is fitted over increasingly large ranges of temperatures. As a result, the top-level overestimates the value at which the resistance should be after the sudden transition, resulting in an inflection point with a positive bias. Overall, as the sigmoidal function is monotonically increasing, a correction would cause a leftward shift in our predicted transition temperature, thus moving it closer to the temperature predicted by the Meissner Effect experiment. This error could be reduced by either choosing a different fit family which includes a sudden increase, but still has change at the wings, like $\tan^{-1} x$, or taking a larger sample of data points near the transition temperature, and fitting the sigmoidal curve to only those points, to decrease the amount of positive bias arising from increasing resistance with temperature.

Another interesting point to note was the non-zero resistance of the samples below the superconducting point at all currents tested. As the resistance of the sample is very low, this could be attributed to two sources: the

resistance of the wires, however small, used to connect to the voltmeter, and impurities in the tin-lead alloy, which would have decreasing resistance with decreasing temperature, as seen in the data points below the transition temperature.

VI. CONCLUSION

In this experiment, we successfully illustrated the fundamental phenomena definitive of superconductors and determined some of the superconducting properties of a sample with unknown conducting behavior. For the pure metals (Pb, In, and Sn), all of our critical temperature and critical field predictions were consistent with values found in the literature. The critical field values for In_2Bi and the critical temperature and field values for In_4Bi were not found in the literature, but the reduced-chi-squared values of the functions used to fit their corresponding data lead us to trust the predictions listed in Table I. For SnPb, the sample with unknown conducting behavior, we found its resistance to drop to zero below about $7 - 7.5$ K , and we found a clear critical field value of $H_c(0) \simeq 790$ G.

Acknowledgments

The authors are grateful to Joe Peidle for his assistance throughout the experiment. They are particularly appreciative of his daily help with pre-cooling the samples and with understanding the various apparatus for signal manipulation and data collection.

[1] W. M. Haynes, *CRC handbook of chemistry and physics*. CRC press, 2014.

[2] H. K. Onnes, "The resistance of pure mercury at helium temperatures," *Commun. Phys. Lab. Univ. Leiden*, vol. 12, no. 120, p. 1, 1911.

[3] W. Meissner and R. Ochsenfeld, "Ein neuer effekt bei eintritt der supraleitfähigkeit," *Naturwissenschaften*, vol. 21, no. 44, pp. 787–788, 1933.

[4] F. London and H. London, "The electromagnetic equations of the supraconductor," in *Proceedings of the Royal Society of London A: Mathematical, Physical and Engineering Sciences*, vol. 149, pp. 71–88, The Royal Society, 1935.

[5] V. Ginzburg, "On the theory of superconductivity," *Zh. eksper. teor. Fiz.*, vol. 20, pp. 1064–1082, 1950.

[6] J. Bardeen, L. N. Cooper, and J. R. Schrieffer, "Theory of superconductivity," *Physical Review*, vol. 108, no. 5, p. 1175, 1957.

[7] F. Behroozi, "Magnetic behavior of superconductors: An experiment for the advanced laboratory," *Am. J. Phys*, vol. 51, no. 1, pp. 28–32, 1983.

[8] U. S. N. B. of Standards and F. G. Brickwedde, *The" 1958 He4 Scale of Temperatures."*. 1960.

[9] M. Tinkham, *Introduction to superconductivity*. Courier Corporation, 1996.

[10] P. R. Bevington and D. K. Robinson, "Data reduction and error analysis," *McGraw-Hill*, 2003.

[11] "scipy.optimize.curvefit," March 2016.